Size classification of silicon nanocrystals

Renato P. Camata,[a] Harry A. Atwater, and Kerry J. Vahala
Thomas J. Watson Laboratory of Applied Physics, California Institute of Technology, Pasadena, California 91125

Richard C. Flagan
Department of Chemical Engineering, California Institute of Technology, Pasadena, California 91125

(Received 9 February 1996; accepted for publication 22 March 1996)

We report on the synthesis of size-classified silicon nanocrystals by differential mobility classification of a polydisperse ultrafine silicon aerosol. Using the described technique, the average nanocrystal size can be tuned by simply adjusting an electric field. Samples of nonagglomerated silicon nanocrystals have been obtained and size control has been achieved within 15%–20% in the 2–10 nm size regime. © *1996 American Institute of Physics.* [S0003-6951(96)04422-1]

Visible luminescent group IV nanostructured materials such as porous silicon[1] and silicon and germanium nanocrystals[2,3] are potential candidates for silicon-compatible optoelectronic devices. Although these nanostructured materials have been the subject of numerous studies, the mechanism of visible luminescence has not yet been completely established. Models involving quantum confinement of excitons and interface electronic states have been proposed in attempts to explain this phenomenon.[4–6] Quantum confinement should in principle lead to size-dependent luminescence spectra, if this is the dominant mechanism for photocarrier recombination.[7,8] Experimental confirmation of this mechanism requires that measurements be made either on single nanocrystals or ensembles having carefully controlled sizes. Although size classification of silicon nanocrystals has been achieved to a certain extent by size-selective chemical precipitation,[4] as also demonstrated for II–VI semiconductor crystallites,[9] most of the studies to date have involved samples with broad size distributions containing large chains of nanostructures, thereby complicating the interpretation of the luminescence behavior.[5,6] In this letter, we demonstrate the generation of nearly monodisperse, nonagglomerated silicon nanocrystals via aerosol routes. These nanocrystals can potentially be used in optical experiments and help clarify the luminescence mechanism.

The experimental apparatus used in this work contains five elements: a nanocrystal source, an aerosol neutralizer, a size classifier, an aerosol concentration monitor, and a collection device. These elements are arranged as shown in Fig. 1. Their functions are summarized as follows.

The silicon nanocrystals are produced in the form of an aerosol by direct ablation or evaporation of crystalline silicon substrates in a high-voltage electric spark discharge.[10] Research purity argon (99.9995% min) further cleaned with a gas purifier is used as carrier gas for the nanocrystals. Voltage, current, frequency, and diluent flow rate in the spark discharge region are adjusted to generate an ultrafine aerosol in 1–10 nm size range. The initial charge state of this aerosol is not well known. A known distribution is imparted on the aerosol by exposing it to ionizing radiation from a sealed Kr^{85} β source. Reactions with the ambipolar gas ions in this ''neutralizer'' result in a steady-state charge distribution with respect to nanocrystal size which has been predicted by Fuchs.[11]

Downstream from the neutralizer, the nanocrystal aerosol is classified with a radial differential mobility analyzer (RDMA).[12] The RDMA is the aerodynamic analog of a dispersive mass spectrometer. Physically, this instrument is a parallel plate capacitor with radial symmetry in which the positively charged nanocrystals migrate across an inward radial laminar flow of sheath gas as a result of an electric field. Because the nanocrystal mobility is a function of its projected area, nanocrystals with different sizes have distinct trajectories inside the RDMA. A sampling orifice suitably placed at the center of the analyzer extracts only nanocrystals in a narrow window of sizes. By varying the voltage across the capacitor, the applied field is varied and the size of the classified nanocrystals can be continuously tuned. Short resi-

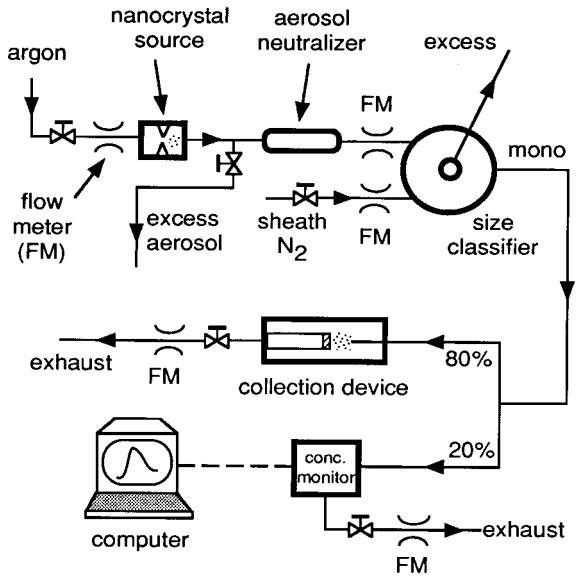

FIG. 1. Schematic of the experimental apparatus for synthesis and size classification of silicon nanocrystals, showing the nanocrystal source, the aerosol neutralizer, the size classifier (radial differential mobility analyzer), the aerosol concentration monitor (electrometer or condensation nucleus counter), and the collection device (hypersonic impactor or electrostatic precipitator).

[a]Electronic mail: rcamata@cco.caltech.edu

 0003-6951/96/68(22)/3162/3/$10.00

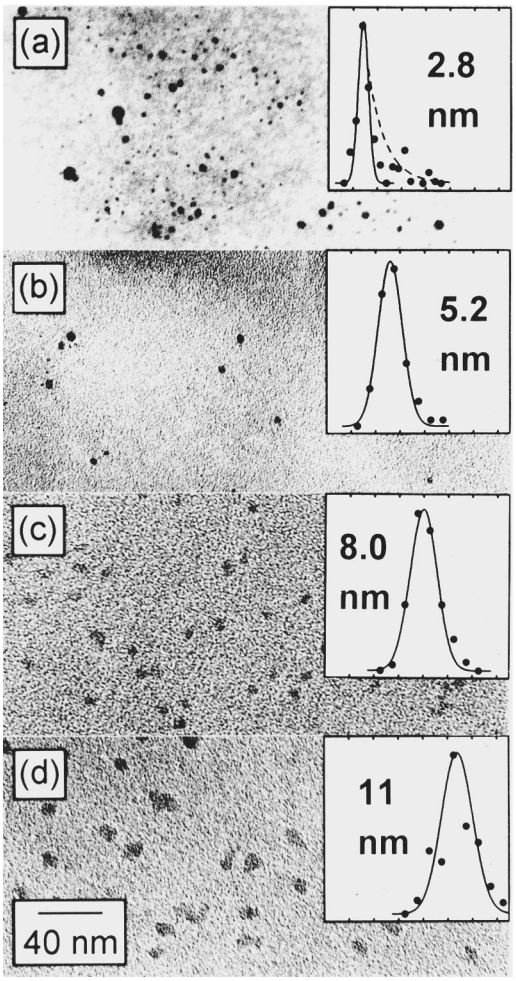

FIG. 2. Bright-field transmission electron micrographs from four samples of silicon nanocrystals on holey carbon substrates. Size classification was aimed at (a) 3.0 nm (10.0 V at the size classifier), (b) 5.0 nm (24.5 V), (c) 7.5 nm (54.1 V), and (d) 10 nm (111 V). The insets show the size distributions determined from the micrographs. The horizontal axis in the insets corresponds to nanocrystal diameter. It begins at zero and the distance between two adjacent ticks is 2 nm. The vertical axis is in arbitrary units and indicates nanocrystal counts from areas larger than shown in the figure. Total nanocrystal counts were 265 in (a), 70 in (b), 166 in (c), and 181 in (d). Gaussian fits to the size distribution data points yield mean diameters of 2.8, 5.2, 8.0, and 11 nm in the samples classified for 3.0, 5.0, 7.5, and 10 nm, respectively.

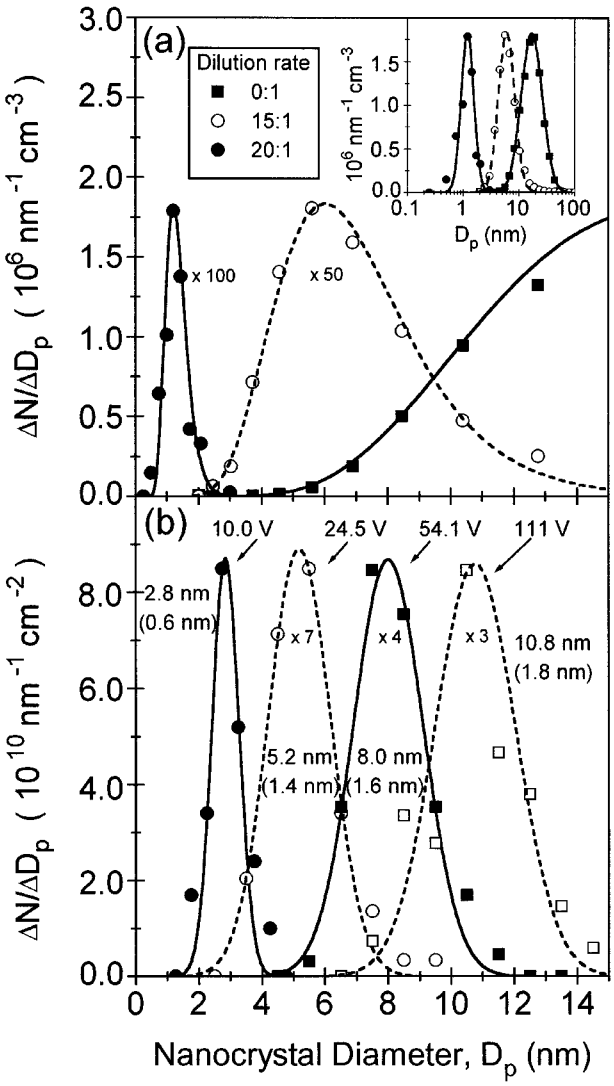

FIG. 3. (a) Nanocrystal size distributions prior to size classification, generated using the size classifier as a spectrometer. Unclassified nanocrystals present log-normal size distributions with geometric standard deviation $\sigma_g \sim 1.4-1.6$. The mean diameter changes with dilution rate. The inset shows same data in log scale. (b) Nanocrystal size distributions after size classification, generated by Gaussian fits to transmission electron microscopy results from Fig. 2. Classified nanocrystals have size distributions with $\sigma_g \sim 1.2-1.3$. Mean diameter, standard deviation (in parentheses), and voltage at the size classifier are shown for each curve. Only the well-defined peak at 2.8 nm shown in the inset in Fig. 2(a) is reproduced here.

dence time and high transmission efficiency of the incoming aerosol in the 3.0–10 nm size range enable the RDMA to classify silicon nanocrystals according to mobility down to sizes relevant to quantum size effects.

The concentration of classified nanocrystals is monitored by taking 20% of its volumetric flow into a femto-ampere sensitivity electrometer or, alternatively, into a condensation nucleus counter.[13] The combined operation of the RDMA and the concentration monitor allows determination of the nanocrystal size distribution, providing information to ensure stable operation of the source.

Most of the classified nanocrystals (80%) are removed from the gas flow and deposited on a substrate. For this purpose, both a hypersonic impactor[14] and an electrostatic precipitator[15] have been used as collection devices. In the hypersonic impactor, the nanocrystals acquire hypersonic speeds as they pass through a nozzle connecting a high pressure region (~760 Torr) to a low pressure region (~1.5 Torr). This causes nanocrystals larger than ~6 nm to impact on a substrate perpendicular to the flow. For nanocrystals smaller than 6 nm, an electrostatic precipitator drives the nanocrystals towards the collection substrate.

The crystalline nature of the particles has been confirmed by electron diffraction and high resolution transmission electron microscopy (TEM). Oxide shells on the nanocrystals have been detected by x-ray photoelectron analysis and high resolution TEM. However, in this letter no attempt is made to distinguish between crystallite size and crystallite-plus-oxide shell size. Therefore, the terms *nanocrystal size* and *nanocrystal diameter* should be understood as the ''nanocrystal'' size and ''nanocrystal'' diameter as resolved from low resolution TEM micrographs or as determined by the RDMA calibration.

To collect a size-classified sample, the RDMA voltage was maintained at a specific value. Classification for different sizes was achieved by changing the RDMA voltage. Figure 2 presents TEM micrographs from samples that have been classified for (a) 3.0 nm, (b) 5.0 nm, (c) 7.5 nm, and (d) 10 nm by RDMA voltages of 10.0, 24.5, 54.1, and 111 V, respectively. Nanocrystals are nonagglomerated and found in concentrations as high as 10^{11} nanocrystals/cm^2. Approximately spherical as well as irregularly shaped nanocrystals are observed. Size distributions obtained from the micrographs are shown in the insets. These distributions represent nanocrystal counts from areas larger than shown in the figure. Total nanocrystal counts were 265 in (a), 70 in (b), 166 in (c), and 181 in (d). Mean diameters of 2.8, 5.2, 8.0, and 11 nm were found in the samples classified for 3.0, 5.0, 7.5, and 10 nm, respectively. The nanocrystal diameters determined by TEM agree within the experimental error with the values predicted by the RDMA calibration.

Although the size distribution in Fig. 2(a) presents a well-defined peak at 2.8 nm, a significant number of larger nanocrystals can be identified in the 5–9 nm range. This result suggests that an important concentration of multiply charged crystallites entered the RDMA. This leads to the sampling of larger nanocrystals along with the targeted ones as the RDMA is a mobility classifier. Supporting evidence for this interpretation comes from the fact that for the particular experiment which led to this result, the aerosol neutralizer had been removed from the setup (Fig. 1) to reduce the nanocrystal loss at these small sizes. Therefore, it is likely that a fraction of nanocrystals possessed more than one elementary charge, partially degrading the size distribution as observed in Fig. 2(a).

Figure 3 compares size distributions before and after classification. In Fig. 3(a) the size distributions before classification were obtained by scanning the RDMA voltage between 1 and 7759 V, thereby probing sizes in the 1–100 nm range. The nanocrystal concentration was measured by the condensation nucleus counter and electrometer at given sizes as determined from the voltage on the RDMA. The spark current was 40 mA and the frequency 120 Hz. These data indicate that unclassified nanocrystals present approximately log-normal size distributions with geometric standard deviation $\sigma_g \sim 1.4-1.6$. The mean diameter of the size distribution can be varied over the 1–20 nm range by adjusting the dilution rate. In Fig. 3(b) Gaussian fits to size distribution data points obtained from the TEM results in Fig. 2 are presented. Classified nanocrystals show size distributions with $\sigma_g \sim 1.2-1.3$. By size classification we have achieved control over mean nanocrystal size within 15%–20% down to a median diameter of 2.8 nm. Figure 3(b) reveals that the size distribution broadens as larger nanocrystals are classified. All size distributions have, however, approximately the same σ_g, indicating consistent operation of the RDMA.

In summary, we have demonstrated the synthesis of samples of nonagglomerated, size-classified silicon nanocrystals in the 2–10 nm size regime. Classified nanocrystal samples were produced by processing polydisperse aerosol through a radial differential mobility analyzer. The resulting deposits of size-classified crystallites may be used in electronic structure characterization experiments and help clarify the luminescence behavior in silicon nanocrystals.

The procedure for size classification described here is applicable to ultrafine particles generated by other vapor phase methods, e.g., pulsed laser ablation or chemical vapor deposition. These techniques may be combined with differential mobility size classification to improve size control of nanocrystal samples.

This work was supported by the U.S. Department of Energy (Grant DE-FG 89ER45395) and by the Office of Naval Research (Grant N00014-90-J-1854). R. P. C. acknowledges support from CNPq, Brasília, Brazil.

[1] L. T. Canham, Appl. Phys. Lett. **57**, 1046 (1990).
[2] Y. Maeda, N. Tsukamoto, Y. Yazawa, Y. Kanemitsu, and Y. Matsumoto, Appl. Phys. Lett. **59**, 3168 (1991).
[3] H. A. Atwater, K. V. Shcheglov, S. S. Wong, K. J. Vahala, R. C. Flagan, M. L. Brongersma, and A. Polman, Mater. Res. Soc. Symp. Proc. **316**, 409 (1994).
[4] W. L. Wilson, P. F. Szajowski, and L. E. Brus, Science **262**, 1242 (1993).
[5] S. Schuppler, S. L. Friedman, and M. A. Marcus, Phys. Rev. B **52**, 4910 (1995).
[6] W. E. Carlos and S. M. Prokes, J. Vac. Sci. Technol. **13**, 1653 (1995).
[7] T. Takagahara and K. Takeda, Phys. Rev. B **46**, 15578 (1992).
[8] B. Delley and E. F. Steigmeier, Phys. Rev. B **47**, 1397 (1993).
[9] C. B. Murray, D. J. Norris, and M. G. Bawendi, J. Am. Chem. Soc. **115**, 8706 (1993).
[10] W. A. Saunders, P. C. Sercel, R. B. Lee, H. A. Atwater, K. J. Vahala, R. C. Flagan, and E. J. Escorcia-Aparcio, Appl. Phys. Lett. **63**, 1549 (1993).
[11] A. Wiendensohler, J. Aerosol Sci. **19**, 387 (1988).
[12] S.-H. Zhang, Y. Akutsu, L. M. Russell, R. C. Flagan, and J. H. Seinfeld, Aerosol Sci. Technol. **23**, 357 (1995).
[13] J. Kesten, A. Reineking, and J. Porstendorfer, Aerosol Sci. Technol. **15**, 107 (1991).
[14] J. Fernandez de la Mora, S. V. Hering, N. Rao, and P. H. McMurray, J. Aerosol Sci. **21**, 169 (1990).
[15] See, for example, Y.-S. Cheng, H.-C. Yeh, and G. M. Nanapilly, Am. Ind. Hyg. Assoc. J. **42**, 605 (1981).